communications earth & environment

ARTICLE

https://doi.org/10.1038/s43247-023-00989-x OPEN

Electron flux is a key determinant of uranium isotope fractionation during bacterial reduction

Ashley R. Brown [1], Margaux Molinas[1], Yvonne Roebbert[2], Ataru Sato[3], Minori Abe[3,4], Stefan Weyer[2] & Rizlan Bernier-Latmani [1✉]

Uranium isotopic signatures in the rock record are utilized as a proxy for past redox conditions on Earth. However, these signatures display significant variability that complicates the interpretation of specific redox conditions. Using the model uranium-reducing bacterium, *Shewanella oneidensis* MR-1, we show that the abundance of electron donors (e.g., labile organic carbon) controls uranium isotope fractionation, such that high electron fluxes suppress fractionation. Further, by purifying a key uranium-reducing enzyme, MtrC, we show that the magnitude of fractionation is explicitly controlled by the protein redox state. Finally, using a mathematical framework, we demonstrate that these differences in fractionation arise from the propensity for back-reaction throughout the multi-step reduction of hexavalent uranium. To improve interpretations of observed fractionations in natural environments, these findings suggest that a variable intrinsic fractionation factor should be incorporated into models of uranium isotope systematics to account for differences in electron flux caused by organic carbon availability.

[1] École Polytechnique Fédérale de Lausanne (EPFL), Environmental Microbiology Laboratory, CH-1015 Lausanne, Switzerland. [2] Institute of Mineralogy, Leibniz University Hannover, D-30167 Hannover, Germany. [3] Department of Chemistry, Tokyo Metropolitan University, Tokyo, Japan. [4] Department of Chemistry, Hiroshima University, Hiroshima, Japan. ✉email: rizlan.bernier-latmani@epfl.ch

Uranium isotopic signatures are increasingly employed as a redox proxy of ancient oceanic and atmospheric conditions[1–4]. Their use hinges on the understanding that hexavalent uranium (U^{VI}) to tetravalent uranium (U^{IV}) redox transitions, mediated by either abiotic reductants or via enzymes, typically result in permil-level fractionations of the two most abundant U isotopes[1]. Here, the heavy ^{238}U is expected to preferentially accumulate in the reduced U^{IV} product, with the light ^{235}U enriched in the U^{VI} reactant. This mass-independent fractionation, the opposite of that expected for light elements, has been observed in both laboratory experiments[5–9] and nature[2–4,10–13]. The observed direction of U isotope fractionation is typically in agreement with ab initio calculations of fractionation at equilibrium. This occurrence is due to the dominance of the nuclear volume term that accounts for the distortions imparted by heavy nuclei's sizes and shapes on electron densities, the so-called nuclear field shift effect[14–18].

However, U isotope signatures and their associated fractionation factors (ε) display significant variability that complicates the interpretation of specific redox conditions. For example, the magnitude of ε is impacted by the chemical reductant type[8], the bacterial species[6], the U supply rate[5], and U speciation[7]. Indeed, cases of dominantly mass-dependent fractionation (operating for U in the opposite direction to that predicted by nuclear field shift theory) have also been reported for both biotic[19] and abiotic reactions[8]. Hence, it remains challenging to reliably interpret U isotopic fractionation signatures. Despite this, current models of U isotope systematics in anoxic basins typically apply an invariant "intrinsic" fractionation factor, based on experimental evidence or ab initio calculation of full equilibrium, in addition to a diagenetic control, i.e., the balance between the rates of U^{VI} delivery to the sediment-water interface and reduction[11,20–22]. Robust reconstructions of both modern and paleo redox conditions would require a mechanistic understanding of the factors controlling the variability in U isotope fractionation factors.

Microbial reduction of U^{VI} is widespread in the environment and has been implicated as a major driver of U isotope fractionation in both pristine and engineered environments[10,23–25]. A metabolically diverse array of bacteria is capable of U^{VI} reduction, with the dissimilatory metal- and sulfate-reducing bacteria being amongst the best studied[26]. Members of these groups have been shown to reduce U^{VI} with electrons released from the oxidation of an electron donor (e.g., lactate, acetate, formate, or H_2). The electrons are transported along the electron transport chain via a series of enzymes with increasing electrochemical potentials. For instance, in the metal-reducing bacterium *Shewanella oneidensis* MR-1, the electron transport terminates at the outer membrane, where outward-facing membrane-associated *c*-type cytochromes are localized and U^{VI} reduction occurs primarily[27,28] (Fig. 1). Successive heme iron centers (Fe_{heme}) within the protein scaffold act as a redox conduit, facilitating the transfer of electrons across the cellular membrane to the electron acceptor, which in the case of U^{VI}, requires two electrons for full reduction to U^{IV} [26–28].

Recent research has implicated reaction rate as a primary determinant of U isotope fractionation during bacterial U^{VI} reduction[5]. This model considers diffusional limitations in the relative supply of the two isotopes to the cellular membrane as the source of fractionation and applies an invariant "intrinsic" fractionation factor, which is fully expressed when U supply is not limiting. Additionally, a recent model of kinetic isotope fractionation that incorporates Marcus theory of electron transfer has been used to describe a linear relationship between reaction free energy (and hence, according to Marcus theory, reaction rates) of two abiotic reaction partners and observed kinetic fractionation factors[29]. However, reaction rates in bacteria are not governed solely by U substrate supply, or reaction free energy. Several studies have shown that the rate of extracellular electron transfer is also impacted by the type and availability of the electron donor, where the release of electrons requires multiple reaction steps and involves a multitude of redox partners[30–34]. Hence, the above models do not account for the impact that electron flux through the electron transport chain may have on the observed isotope fractionation.

To explore the mechanism of control of the reaction rate over isotope fractionation, reaction kinetics, and associated isotope fractionation during U^{VI}-citrate reduction by *S. oneidensis* were assessed. Using a mathematical framework first established for microbial sulfur fractionation[35–37], we show that the magnitude of fractionation is controlled by the flux of electrons from metabolism. Additionally, we report the U isotope signatures for reduction by a purified *c*-type cytochrome from *S. oneidensis*, MtrC, at different redox states, allowing us to make the link between molecular level fractionations at the redox interface and observed fractionations in natural environments.

Results and Discussion

Reaction rate and uranium isotope fractionation. Previous studies suggest that reaction rate may control observed isotope fractionation[5,7,29,38]. We tested this hypothesis by impacting global reaction rates of the biological reduction of U^{VI}-citrate through the systematic modulation of *S. oneidensis* MR-1 biomass (Fig. 2a). Despite significant differences in reaction rates ($k = 0.013\text{-}0.364\ h^{-1}$), only negligible differences between fractionation factors were observed (Fig. 2b), suggesting that the reaction rate (k) does not inherently control fractionation. Indeed, Joe-Wong and Maher[29] suggest a relationship between reaction free energy ($\Delta G_r°$) and kinetic isotope fractionation (ε^{kin}), aimed at abiotic redox reactions and through a theoretical model incorporating Marcus theory of electron transfer. Despite its biological nature, the results in our system are in agreement with the Joe-Wong model. As the initial U speciation remained the same across all conditions, initial reaction free energy was also the same in each system, regardless of differing biomass concentrations. Thus, the model would predict that the fractionation factors would remain the same, which is what was observed.

A multi-step model of reduction and isotopic fractionation of U-citrate. An alternative model of microbial U^{VI} reduction has presented a framework of fractionation during multi-step U^{VI} reduction (including a pentavalent U (U^{V}) intermediate) under steady-state conditions[37], based on the one first described for fractionation of sulfur isotopes during microbial dissimilatory sulfate reduction[35,36]. This model expresses observed fractionation (that can be described by a Rayleigh distillation model ($\varepsilon^{Rayleigh}$)) in terms of equilibrium isotope fractionation coefficients (ε^{eq}) for each reaction step. This analysis, using ab initio calculations of ε^{eq} and comparison to experimentally determined $\varepsilon^{Rayleigh}$ for bacterial U^{VI} reduction, revealed that one or several reaction steps must involve a kinetic isotope fractionation component (ε^{kin}) to account for non-equilibrium conditions.

Indeed, when thermodynamic equilibrium is reached and the forward and backward fluxes are equal, the equilibrium isotope effect can be described as the difference between the kinetic fractionation of the forward reaction and that of the backward reaction[35]. On the other hand, when the forward reaction is greater than the backward reaction, the full equilibrium fractionation is not expressed, as shown in previous studies[35–37]. In the latter case, the total observed fractionation can be described by modulating the relative expression of the kinetic fractionation terms to account for varying extents of forward and backward reaction[35–37]. Therefore, unidirectional or irreversible reaction

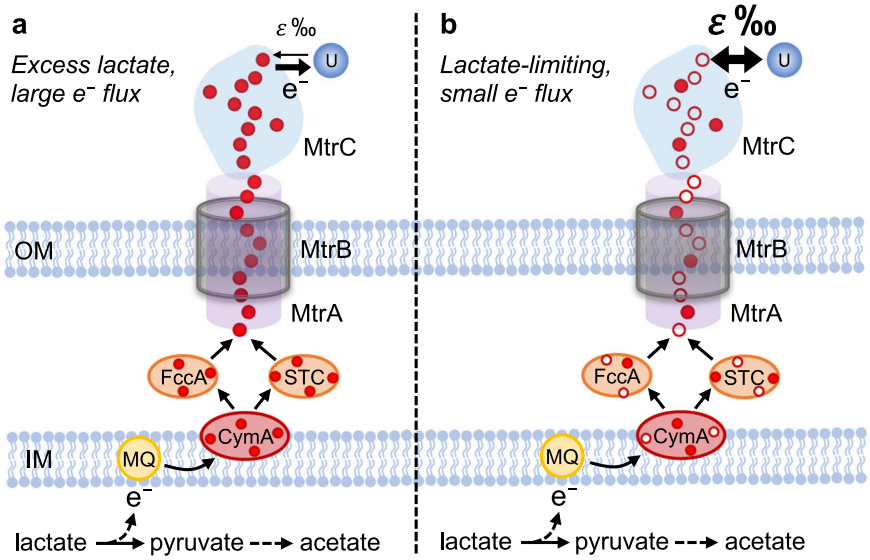

Fig. 1 Schematic of the electron transport chain in *S. oneidensis* MR-1. a Electron transport for excess lactate conditions with a large electron flux. **b** Electron transport for lactate-limiting conditions with a small electron flux. Red circles represent heme iron centers in either their reduced state (solid fill) or oxidized state (open fill). Dotted lines represent metabolic pathways in which the intermediaries have been removed for simplicity. OM outer membrane, IM inner membrane, MQ menaquinone. CymA, FccA, STC (small tetraheme cytochrome), MtrA, MtrB, and MtrC are redox active multi-heme cytochromes.

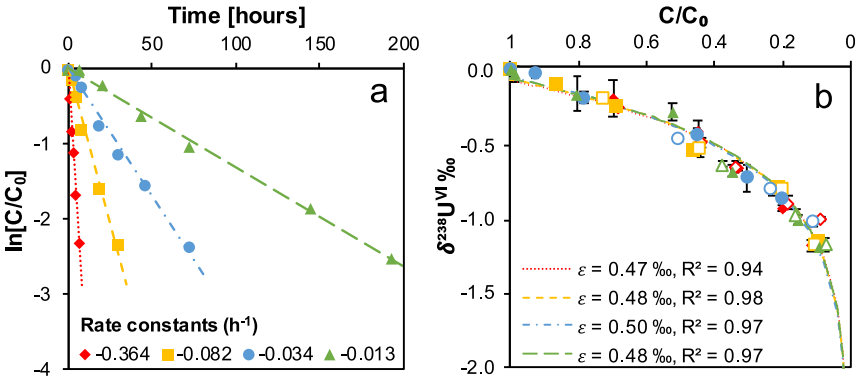

Fig. 2 The impact of biomass concentration on U^{VI} reduction rates and isotopic fractionation. a Mean concentration of U^{VI}, as a function of time, in duplicate reactors containing U^{VI} citrate incubated with varying concentrations of *S. oneidensis* MR-1 (in 10^8 cells mL^{-1}: green triangle, 0.23; blue circle, 0.7; yellow square, 2.3; red diamond, 11). Values are plotted as the natural logarithm of the fraction of U^{VI} remaining and dashed lines depict linear regressions of the mean values from which the first-order reaction rate is derived. **b** $\delta^{238}U$ values for U^{VI} reported as a function of the remaining U^{VI} fraction. Each symbol shape represents the same treatments as for panel (**a**), with open and filled symbols representing duplicate reactors. Rayleigh model curves for the combined reactor data are shown with dashed lines, along with their corresponding isotope enrichment factors (ε) and the R^2 of the Rayleigh fit. Error bars depict two standard deviations of the mean of triplicate measurements. Where not visible, the error is smaller than the symbol size.

steps do not express the full fractionation predicted at equilibrium, whereas fully reversible reaction steps (at equilibrium) exhibit the full equilibrium fractionation factor. The implication here is that conditions permitting the back-reaction should show higher levels of fractionation than those in which the back-reaction is limited (either thermodynamically or kinetically).

Here, we consider a multi-step reaction for the reduction of U^{VI}-citrate, supposing the following reaction scheme:

transfers, and finally resulting in the release of U^{IV} from MtrC. Here, we present the ligand as remaining bound to U throughout the reaction since U remains in the aqueous phase throughout the reaction (Supplementary Fig. 1) suggesting strong complexation by citrate. Likewise, recent research has shown that two successive electron transfers are the predominant mechanism in the presence of a strong organic complexing agent[39], as opposed to a single electron transfer followed by disproportionation of U^{V}

$$\underset{A}{U^{VI}cit.} + MtrC \rightleftharpoons \underset{B}{U^{VI}cit.MtrC} \rightleftharpoons \underset{C}{U^{V}cit.MtrC^{+}} \longrightarrow \underset{D}{U^{IV}cit.MtrC^{++}} \longrightarrow \underset{E}{U^{IV}cit.} + MtrC^{++} \quad (1)$$

where MtrC represents the terminal *c*-type cytochrome reductase on the outer membrane of *S. oneidensis*. The first step represents the binding of U^{VI} to MtrC, followed by two successive electron intermediaries[40]. Additionally, steps C to D and D to E are represented as being irreversible as the oxidation of U^{IV}-citrate by oxidized MtrC does not occur[41].

Here, we consider the heme Fe centers (Fe_{heme}) of the initial MtrC to be fully reduced prior to interaction with U^{VI} and, for ease of representation, we present this fully reduced state without a charge. As the reduction proceeds to U^{IV}, two of the MtrC Fe_{heme} are oxidized (delivering two electrons) and the charge of MtrC is expressed as $MtrC^{++}$ at the end of the reaction.

The reaction scheme can be simplified and the forward and backward reactions for each reaction step are expressed as a flux (N), such that N_{ab} describes the forward reaction flux between reactants A and product B; and N_{ba} describes the backward reaction flux from the product (B) to the initial reactants (A):

$$\begin{matrix} & N_{ab} & N_{bc} & N_{cd} & N_{de} & \\ A & \rightleftharpoons & B & \rightleftharpoons & C \rightarrow D \rightarrow E \\ & N_{ba} & & N_{cb} & & \end{matrix} \quad (2)$$

Thus, the forward and backward reaction flux ratios (X) can be expressed as follows:

$$X_b \equiv \frac{N_{ba}}{N_{ab}} \text{ and } X_c \equiv \frac{N_{cb}}{N_{bc}} \quad (3)$$

$$\widetilde{X}_b = 1 - X_b \text{ and } \widetilde{X}_c = 1 - X_c \quad (4)$$

where $X = 1$, $\widetilde{X} = 0$, represents equilibrium; and $X = 0$, $\widetilde{X} = 1$, represents an irreversible reaction.

The calculation of $\varepsilon^{Rayleigh}$ can be formulated as for Sato et al. [37]:

$$\varepsilon^{Rayleigh} = \left(\varepsilon^{eq}_{ab} + \varepsilon^{kin}_{ba}\widetilde{X}_b\right) + \left(\varepsilon^{eq}_{bc} + \varepsilon^{kin}_{cb}\widetilde{X}_c\right)X_b + \varepsilon^{kin}_{cd}X_bX_c \quad (5)$$

Here, ε^{eq} represents the equilibrium fractionation factor for each reaction step, which is positive in value as it is predicted to be dominated by the nuclear field shift effect. Additionally, the kinetic fractionation factors for the back-reactions, e.g., ε^{kin}_{ba}, are expected to be negative in value, as explained by Sato et al. [37].

The impact of binding on U isotope fractionation. The first term in Eq. 5 describes the binding of U^{VI} to the cytochrome, MtrC. To determine the contribution of any fractionation from this step to the overall observed fractionation ($\varepsilon^{Rayleigh}$), we first reacted U^{VI} under different concentrations of citrate and MtrC (in its fully oxidized state) to systematically impact binding extent without reduction (Supplementary Fig. 2). Negligible fractionation was observed after 1 h of reaction, suggesting that this step does not contribute to overall observed fractionation factors within the time frame of reduction by whole bacterial cells. Given that U isotope fractionation is predominantly associated with redox changes and given that binding does not impact the redox state of U, this result is to be expected. However, it is not evident from these data whether ε^{eq}_{ab} and ε^{kin}_{ba} are small in magnitude, or whether this reaction is far from equilibrium (X_b « 1 and hence, $\widetilde{X}_b$ >> 0) and ε^{kin}_{ba} is negative in value, canceling out ε^{eq}_{ab}. Despite these unknowns, it is apparent that the first term contributes negligible fractionation, allowing Eq. 5 to become:

$$\varepsilon^{Rayleigh} \approx \left(\varepsilon^{eq}_{bc} + \varepsilon^{kin}_{cb}\widetilde{X}_c\right)X_b + \varepsilon^{kin}_{cd}X_bX_c \quad (6)$$

The impact of electron donor concentrations on U isotope fractionation. Next, we investigated the contribution of fractionation at the electron transfer steps. Specifically, we sought to explore the importance of X_c (and $\widetilde{X}_c$) in regulating observed fractionation factors by reacting U^{VI}-citrate with *S. oneidensis* MR-1 over a range of electron donor (i.e., lactate) concentrations. Here, we hypothesized that systems in which the lactate concentration limits electron flux through the electron transport chain should show more fractionation because the back-reaction from U^{V} (C to B) may be more extensive (X_c >> 0 and hence, $\widetilde{X}_c$<< 1) (Fig. 1b). That is to say, electron transfer from U^{V} to Fe_{heme} of multi-heme cytochromes on the bacterial surface may be more likely, as all Fe_{heme} may not be reduced under lactate-limiting conditions. Such back-reaction would be expected to permit the preferential accumulation of the heavier ^{238}U in the reduced product (as predicted by the nuclear field shift effect at equilibrium), where it is thermodynamically more favorable than the lighter ^{235}U. In mathematical terms in the steady-state model (Eq. 6), if $\widetilde{X}_c$<< 1, the contribution of the reverse kinetic term (ε^{kin}_{cb}) would be limited and thus, the expression of the equilibrium terms (ε^{eq}_{bc}) would not be diminished significantly.

Conversely, we hypothesize that lactate-replete systems would have a higher flux of electrons to the membrane-located proteins, and hence Fe_{heme} would be readily re-reduced upon delivery of an electron, preventing electron transfer from reduced U species to hemes (Fig. 1a). Thus, limited back-reaction would hinder the preferential reduction of the heavier ^{238}U, i.e., reduction of both U isotopes would be closer to quantitative, and less fractionation would be observed. In terms of the steady-state model (Eq. 6), this irreversibility (X_c << 1 and hence, $\widetilde{X}_c$ >> 0) would lead to an increased contribution of the reverse kinetic term (ε^{kin}_{cb}) and thus, preclude the full expression of the equilibrium term (ε^{eq}_{bc}).

Here, we show that at concentrations at or below 0.5 mM, lactate supply or metabolism becomes rate limiting and U^{VI} reduction rates are correlated with lactate concentration (Fig. 3a). Additionally, observed isotope fractionation factors are also correlated with lactate concentrations (Fig. 3b), and likewise with reaction rates (Fig. 3c), such that, slower reactions resulted in more observed fractionation. These data are consistent with the trend observed previously by Basu et al. [5] and support our hypothesis that electron flux from lactate to the site of U^{VI}-reduction exerts control over fractionation.

The role of the electron transport chain in U isotope fractionation. To further investigate the role of the intracellular electron flux to the membrane cytochromes, cell integrity was disrupted by preparing cell-free extracts of *S. oneidensis* MR-1. These extracts have been shown previously to be capable of U^{VI}-reduction and extensive isotopic fractionation associated with that reduction confirmed the role of redox-active enzymes within the extracts as the source of fractionation[8]. Beyond the absence of a membrane, cell-free extracts differ fundamentally from cells in that they lack an electron transport chain, precluding the replenishment of enzymes with electrons as they become more oxidized. Hence, we hypothesize that, in the absence of an electron transport chain, the electron flux would be limited. Thus, as enzymes deliver electrons that are not replenished, back-reactions would readily occur, resulting in substantial fractionation. UV-Vis spectroscopy confirmed the presence of *c*-type cytochromes (Fig. 4a) and comparison with the oxidized and reduced spectra of the purified MtrC suggests that the cytochrome components of the cell-free extract were not fully reduced.

The reaction of cell-free extract with U^{VI}-citrate was slow, on the order of tens of days (Fig. 4b), compared to that of whole cells of *S. oneidensis* MR-1 (days). As expected, isotope signatures revealed considerable isotopic fractionation (~1 ‰; Fig. 4c), which was much higher than for previous experiments carried out with whole cells (~0.5 ‰ with lactate in excess). Again, these data are consistent with the hypothesis that electron flux may act as a major determinant of fractionation and further point toward the importance of the redox state of the terminal reductase proteins in determining the magnitude of isotope fractionation.

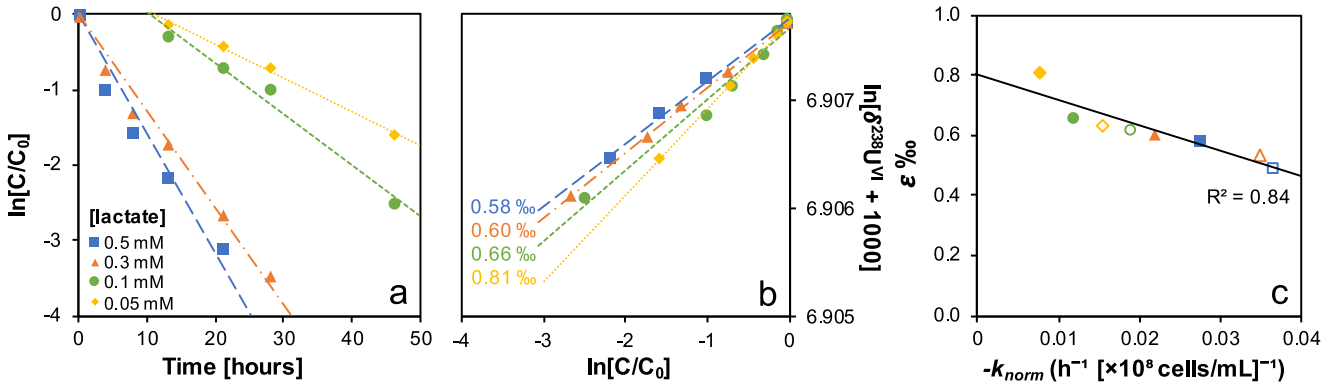

Fig. 3 The impact of electron donor concentration on U^{VI} reduction rates and isotopic fractionation. a Concentration of U^{VI}, as a function of time, in reactors containing U^{VI} citrate incubated with *S. oneidensis* MR-1 and varying concentrations of lactate. Values are plotted as the natural logarithm of the fraction of U^{VI} remaining and solid lines depict linear regressions for each reactor from which first-order rates were calculated (Supplementary Table 1). Systems containing 0.1 or 0.05 mM lactate displayed a lag phase in the onset of reduction and the data from this phase have been excluded from the linear regressions. **b** Linearized plots of isotope signatures, as a function of reaction progression, for reactors containing U^{VI} citrate incubated with *S. oneidensis* MR-1 at different concentrations of lactate. Each symbol shape represents the same treatments as for panel (**a**) and linear regressions represent Rayleigh distillation models and their corresponding isotope enrichment factors (ε). Full details of the models and their R^2 values can be found in Supplementary Table 2. For ease of visualisation, only the data and models for one single experiment are displayed, and the isotope signatures and Rayleigh models for the second replicate are displayed in Supplementary Fig. 8. **c** The correlation between isotope enrichment factors (ε) and rate constants (normalised to reactor cell concentrations). Open and filled symbols represent duplicate reactors for the same treatments as in panel (**a**).

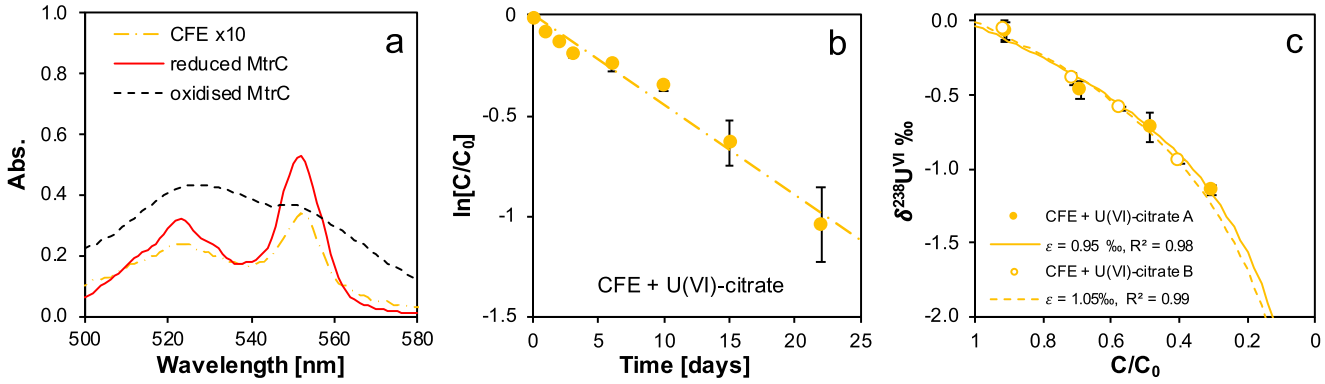

Fig. 4 Reduction and isotopic fractionation of U^{VI} by cell-free extracts of *S. oneidensis*. a Absorbance spectrum of a cell-free extract (CFE) of *S. oneidensis*, displaying peaks at 523 and 552 nm. Spectra of oxidized and sodium dithionite-reduced MtrC are provided for comparison. The CFE spectrum has been multiplied by a factor of 10 for better representation. **b** Concentration of U^{VI}, as a function of time, in reactors containing U^{VI} citrate, incubated with cell-free extracts (CFE) of *S. oneidensis*. Values are plotted as the natural logarithm of the fraction of U^{VI} remaining. Symbols and error bars depict 1 standard deviation of the mean of duplicate reactors and the dashed line depicts the linear regression of the mean values. Where not visible, the error is smaller than the symbol size. **c** $\delta^{238}U$ values for U^{VI} reported as a function of the remaining U^{VI} fraction. Filled and open symbols depict duplicate reactors and error bars show 2 standard deviations of the mean of triplicate measurements. Rayleigh model curves for each duplicate reactor are shown in dashed lines, along with their corresponding isotope enrichment factors (ε).

Reductase redox state and U isotope fractionation. To address the role of reaction reversibility and explicitly examine the control that the redox state of the outer-membrane cytochromes may exert over U isotope fractionation, we systematically varied the redox state of purified MtrC and reacted it with either U^{VI} or U^{IV}. To further simplify the system, we supplied EDTA as the U coordinating ligand as it permits a dominant mononuclear U^{VI} species (Supplementary Fig. 3) under the conditions tested, removing any artifacts from multiple competing species or dynamic speciation changes with decreasing U^{VI} concentrations that are inherent in the U^{VI}-citrate system (Supplementary Figs. 4 and 5).

First, we tested whether reverse electron transfer from U^{IV}-EDTA to oxidized MtrC is possible, allowing us to determine whether a back-reaction between U^{IV}-EDTA and U^{V}-EDTA (corresponding to step D ⟶ C in Eq. 1) can be invoked as a source of isotope fractionation. After 2 h of reaction under anoxic conditions, ~11% of the U^{IV} was oxidized to U^{VI} (Fig. 5a). This was associated with the concomitant reduction of heme groups of MtrC, as evidenced by the emergence of peaks at ~525 and ~550 nm in the UV-Vis spectrum, consistent with that of a chemically reduced MtrC standard (Fig. 5b). These data confirm that the back-reaction is indeed possible, though it is somewhat limited under these conditions.

Second, we followed the reduction and fractionation of U^{VI}-EDTA by a completely reduced MtrC. Full reduction of the heme was achieved by successive additions of sodium dithionite (a potent reductant of Fe_{heme}[42]) until no further change in the UV-Vis spectrum was observed (Fig. 6a). Reduction of U^{VI} was extremely fast (~70% reduction after 3 s; Fig. 6b) and was accompanied by negligible fractionation during this initial phase of the reaction (Fig. 6c and Supplementary Fig. 6). These data indicate that fast reduction results in near-quantitative reduction of U isotopes and suggest a unidirectional reaction with limited

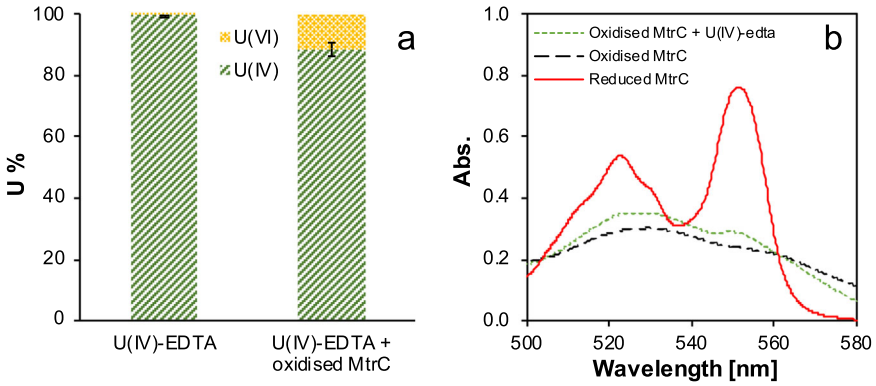

Fig. 5 Electron transfer from U^{IV} to oxidized MtrC. a U oxidation state in reactors with or without the addition of oxidized MtrC. **b** Absorbance spectrum of oxidized MtrC reacted with U^{IV}-EDTA. Spectra of the initial oxidized MtrC and sodium dithionite-reduced MtrC are provided for comparison.

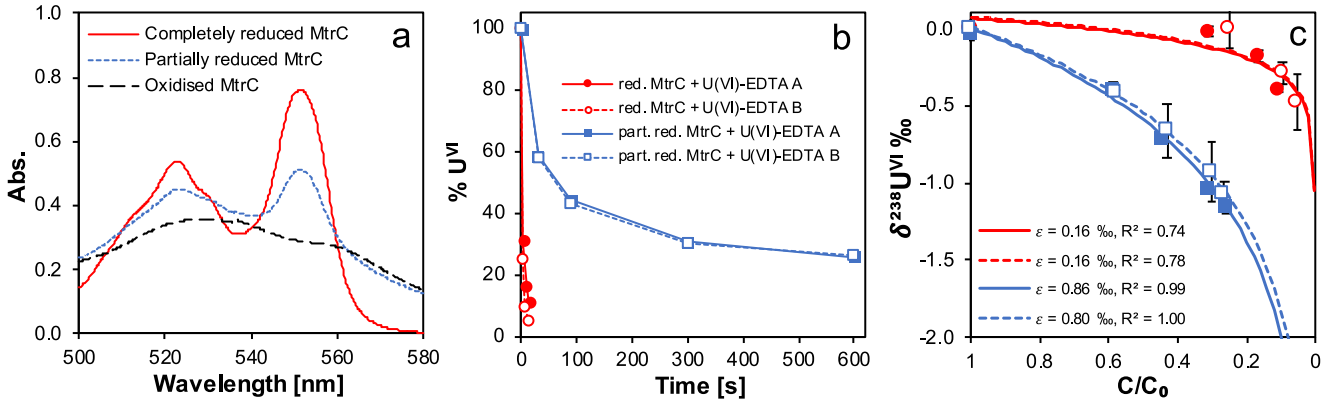

Fig. 6 The impact of MtrC oxidation state on U^{VI} reduction and isotopic fractionation. a Absorbance spectra of *completely* or *partially-reduced* MtrC. *Completely reduced* MtrC was achieved via the step-wise addition of sodium dithionite until no further change in the spectrum was observed. *Partially reduced* MtrC was achieved via the addition of approximately 40% of the amount of sodium dithionite supplied to the completely reduced MtrC. The spectrum of oxidized MtrC is provided for comparison. **b** Concentration of U^{VI}, as a function of time, in reactors containing U^{VI}-EDTA and either *completely* or *partially reduced* MtrC. Filled and open symbols depict duplicate reactors. **c** $\delta^{238}U$ values for U^{VI} reported as a function of the remaining U^{VI} fraction. Filled and open symbols depict duplicate reactors and error bars show 2 standard deviations of the mean of triplicate measurements. Rayleigh model curves for each duplicate reactor are shown in dashed lines, along with their corresponding isotope enrichment factors (ε).

back-reaction. As the reaction progresses (>70% reduction), isotope signatures indicate a progressive increase in fractionation that is not described well by a single Rayleigh model (Fig. 6c and Supplementary Fig. 6). This observation is consistent with the hypothesis that progressive oxidation of Fe_{heme} in MtrC leads to less thermodynamically favorable reduction of U^{VI}, which in turn, permits more reverse electron transfer and greater expression of ε^{eq} for the electron transfer steps.

To test this possibility, a partially reduced MtrC was prepared (Fig. 6a) and reacted with U^{VI}-EDTA (Fig. 6b). Here, slower reduction and significantly more fractionation were observed ($\varepsilon = \sim 0.83$ ‰) than for completely reduced MtrC, and was comparable to that observed for whole cells of *S. oneidensis* MR-1 reacted with U^{VI}-EDTA ($\varepsilon = \sim 1$ ‰; Supplementary Fig. 7). These data are consistent with the steady-state model and are representative of a reversible reaction, which permits the preferential accumulation of the heavier ^{238}U in the reduced product.

Electron flux and U isotope fractionation: a mathematical model. Collectively, these data suggest that electron flux to U^{VI} is a major determinant of observed fractionation factors. Here, we discuss these findings within the framework of the steady-state model of U isotope fractionation described above and modified from Sato et al. [37]. First, we consider two opposing conditions: cell cultures with excess vs. limiting lactate concentrations.

Under excess lactate concentrations, electron flux from lactate metabolism along the electron transport chain is large, which results in extensively reduced MtrC and permits rapid electron transfer to U^{VI} (Fig. 1a). This strong thermodynamic driving force prevents the reverse transfer of electrons from reduced U (either U^{V} or U^{IV}) to MtrC because the newly oxidized terminal heme (from electron transfer to U^{VI}) is rapidly re-reduced by electron transfer from the preceding heme further up the electron transfer chain. This results in a strongly unidirectional reaction, in which U^{VI} reduction is near-quantitative, with a limited preferential reduction of ^{238}U.

Conversely, under low lactate conditions, electron supply to the outer membrane is limited and MtrC is only partially reduced. Now, reverse electron transfer from reduced U back to MtrC is possible because the newly oxidized heme is not immediately re-reduced by an electron from the preceding heme (Fig. 1b). As, according to the nuclear field shift theory, the heavier ^{238}U has a preference for the reduced U^{IV} species, re-oxidation of ^{235}U is more likely[43], resulting in the preferential accumulation of ^{238}U in the reduced product and the expression of larger magnitude fractionation factors.

Distinct reaction pathways can be formulated for these two conditions. The first, for MtrC that is fully reduced initially

(*MtrC*), is representative of cells in excess lactate conditions (Eq. 7). This formulation is similar to Eq. 1 for U^{VI}-citrate, except for the representation of steps C ⟶ D, and D ⟶ E as being reversible (as evidenced above for U-EDTA). Here, L denotes the U-coordinating ligand.

$$\underset{A}{LU^{VI}} + MtrC \rightleftharpoons \underset{B}{LU^{VI}MtrC} \rightleftharpoons \underset{C}{LU^{V}MtrC^{+}} \rightleftharpoons \underset{D}{LU^{IV}MtrC^{++}} \rightleftharpoons \underset{E}{LU^{IV}} + MtrC^{++} \quad (7)$$

As before, the reaction scheme is simplified, and the flux terms are expressed as follows:

$$\begin{matrix} & N_{ab} & N_{bc} & N_{cd} & N_{de} & \\ A & \rightleftharpoons & B & \rightleftharpoons & C & \rightleftharpoons & D & \rightleftharpoons & E \\ & N_{ba} & N_{cb} & N_{dc} & N_{ed} & \end{matrix} \quad (8)$$

Now, the calculation of $\varepsilon^{Rayleigh}$ can be formulated as before, but with the additional terms accounting for the reversibility of the later reaction steps:

$$\begin{aligned} \varepsilon^{Rayleigh} = &\left(\varepsilon_{ab}^{eq} + \varepsilon_{ba}^{kin}\widetilde{X}_b\right) + \left(\varepsilon_{bc}^{eq} + \varepsilon_{cb}^{kin}\widetilde{X}_c\right)X_b \\ &+ \left(\varepsilon_{cd}^{eq} + \varepsilon_{dc}^{kin}\widetilde{X}_d\right)X_bX_c + \left(\varepsilon_{de}^{eq} + \varepsilon_{ed}^{kin}\widetilde{X}_e\right)X_bX_cX_d \end{aligned} \quad (9)$$

The second condition considers MtrC that is only partially reduced initially ($MtrC^{+}$) and is representative of cells in limiting lactate conditions.

$$\underset{A'}{LU^{VI}} + MtrC^{+} \rightleftharpoons \underset{B'}{LU^{VI}MtrC^{+}} \rightleftharpoons \underset{C'}{LU^{V}MtrC^{++}} \rightleftharpoons \underset{D'}{LU^{IV}MtrC^{+++}} \rightleftharpoons \underset{E'}{LU^{IV}} + MtrC^{+++} \quad (10)$$

The reaction scheme is simplified and represented with the prime notation signifying more extensive oxidation of MtrC than for the high lactate condition:

$$\begin{matrix} & N_{ab}\prime & N_{bc}\prime & N_{cd}\prime & N_{de}\prime & \\ A' & \rightleftharpoons & B' & \rightleftharpoons & C' & \rightleftharpoons & D' & \rightleftharpoons & E' \\ & N_{ba}\prime & N_{cb}\prime & N_{dc}\prime & N_{ed}\prime & \end{matrix} \quad (11)$$

Now, the flux terms for the first reaction step for the two conditions (association of U^{VI} to MtrC) can be expressed as follows:

$$N_{ab} = k_{ab}\left[LU^{VI}\right][MtrC] \quad (12)$$

$$N_{ab}\prime = k_{ab}\prime\left[LU^{VI}\right]\left[MtrC^{+}\right] \quad (13)$$

Assuming that k is the same for both (i.e., binding is not dependent on MtrC redox state), N_{ab}' equals N_{ab}, and hence X_b is equal to X_b'. Thus, the first term of the steady-state model (Eq. 9) remains the same for each condition.

However, because of the smaller thermodynamic driving force under limiting lactate conditions, k_{bc}' for LU^{VI}-$MtrC^{+}$ ⟶ LU^{V}-$MtrC^{++}$ (low lactate; B' ⟶ C') is expected to be smaller than k_{bc} for LU^{VI}-MtrC ⟶ LU^{V}-$MtrC^{+}$ (high lactate, B ⟶ C). Hence, N_{bc}' $< N_{bc}$.

Additionally, as MtrC is expected to be more oxidized in the low lactate condition, k_{cb}' for the reverse reaction LU^{V}-$MtrC^{++}$ ⟶ LU^{VI}-$MtrC^{+}$ (low lactate; C' ⟶ B') is expected to be larger than k_{cb} for LU^{V}-$MtrC^{+}$ ⟶ LU^{VI}-MtrC (high lactate; C ⟶ B) and hence, N_{cb}' > N_{cb}. Such that, for low lactate conditions, smaller k_{bc}' and larger k_{cb}' than for the high lactate condition results in $X_c\prime > X_c$ (Eq. 3) and hence $\widetilde{X}_c\prime < \widetilde{X}_c$ (Eq. 4).

Under low lactate conditions, this maximizes the contribution of the full equilibrium fractionation (ε_{bc}^{eq}) in the second term of Eq. 9. Likewise, the reversibility of this reaction step under low lactate conditions, contributes to the accumulation of fractionation from successive reaction steps, due to the appearance of X_c in later reaction terms of Eq. 9.

Indeed, for rapid re-reduction of MtrC under high lactate conditions, the back-reaction LU^{V}-MtrC ⟶ LU^{VI}-MtrC may even be negligible, and $X_c = 0$ and $\widetilde{X}_c = 1$. The result being that for the first electron transfer, the equilibrium term, ε_{bc}^{eq}, is minimized by the full expression of the backward kinetic term, ε_{cb}^{kin}, and thus, all subsequent terms (all multiplied by X_c) approach zero and no further fractionation is expressed (Eq. 9). Likewise, the third term of Eq. 9 (second electron transfer) would be expected to behave in the same manner, with X_d responding in the same way as for X_c under varying lactate concentrations with EDTA as the ligand.

Collectively, our experimental observations are consistent with the steady-state model of microbial U^{VI} reduction. As this model has its mathematical basis in the Rayleigh equation[37], this framework allows the interpretation of observed fractionation factors in terms of reaction reversibility. Here, we have shown that electron flux from the metabolism of the electron donor, through the electron transfer chain all the way to outer-membrane cytochromes acts as a major determinant of fractionation factors. Further, we suggest that these differences in fractionation arise from the propensity for back-reaction throughout the multi-step reduction of U^{VI}.

Basu et al. [5] related the relative rates of U^{VI} supply and U^{VI} reduction to observed fractionation factors using a reactive transport model. Indeed, differences in the ^{238}U and ^{235}U concentration gradients across a diffusive boundary layer were implicated as the source of fractionation. It was supposed that ^{238}U has a larger concentration gradient when reduction is relatively slow with respect to U supply, resulting in faster reaction rates for ^{238}U, which then preferentially accumulates in the reduced product, in accordance with nuclear field shift theory. Conversely, when reduction is rapid with respect to U supply, reduction is quantitative and fractionation is negligible, because of the absence of differential concentration gradients for the two isotopes.

Our data appear consistent with the concept that reduction rate is important as to whether U reduction is quantitative or not. However, U supply is constant in our experiments, except for its changing concentration throughout ongoing reduction. Despite this, isotope signatures from experiments involving whole cells can still be described by a single Rayleigh model (and hence, a constant $\varepsilon^{Rayleigh}$), even though the model of Basu et al. would predict fractionation to progressively decrease as U supply becomes progressively limited. This suggests that under the conditions tested in our experiment (i.e., U supply is not limiting), the model of Basu et al. may not be applicable.

Likewise, our data appear to be incompatible with a model relating reaction rate (dependent on $\Delta G_r°$) to ε^{kin} using Marcus theory of electron transfer[29]. This model predicts that increases in $\Delta G_r°$ result in faster reactions and less attendant fractionation. However, given the same electron donor (lactate) and U speciation, $\Delta G_r°$ is constant in our systems, yet $\varepsilon^{Rayleigh}$ changes.

Notwithstanding, the reductant, MtrC, consists of multiple heme groups with multiple redox potentials[44] and a differential flux of electrons from an external source (that is to say, the electron donor, lactate, is not the reductant per se). Therefore, this system is not only a multi-step reaction of the oxidant (U), but is also a multi-step electron transfer for the reductant (MtrC). Thus, under our conditions, relating our observations to the linear relationship between reaction free energy and ε^{kin} is challenging. Further, Marcus theory does not distinguish between the sources of fractionation, i.e., mass-dependent fractionation vs. nuclear field shift dependent fractionation[29], and the relative contributions of these two effects to ε^{kin} may vary under varying reaction conditions.

Alternatively, transition state theory (on which the steady-state model is built) permits the forward ε^{kin} (ε_f^{kin}) to be considered as ε^{eq} between the reactants and the transition state and the backward ε^{kin} (ε_b^{kin}), that between the transition state and the products. Likewise, the model expresses the overall $\varepsilon^{Rayleigh}$ in terms of the relative forward and backward ε^{kin} components[18,37,45,46]. This allows relative reaction reversibility, controlled by metabolic electron flux, to be invoked as a source of fractionation and permits the explanation of differences in $\varepsilon^{Rayleigh}$ even when there are no perceived differences in $\Delta G_r°$. It is under these conditions that the application of the steady-state model is optimal, although further work is required to explicitly demonstrate the contribution of the nuclear field shift in kinetic fractionation of U isotopes and examine the factors that control its expression relative to mass-dependent fractionation.

Additionally, our work predicts that the type of electron donor will likely impact fractionation, if the rate and pathway of its oxidation are distinct from that of lactate, e.g., H_2 or formate. Indeed, the electron donor type/concentration effect has been observed previously for sulfur isotope fractionation[35,47], and fractionation factors were explained using reaction reversibility described by the steady-state model[48,49]. Here, using purified MtrC of various redox states, we have provided direct experimental evidence of this phenomenon and suggest that these findings may be extended to other isotope systems that involve multi-step redox transformations and can be described by the steady-state model.

Further, our data also highlight the importance of U speciation in controlling back-reaction (i.e., U-citrate versus U-EDTA), although further work, in tandem with ab initio calculation of ε^{eq} for each species, is required to confirm this.

Environmental and Geological Implications. Current models of U isotope systematics typically consider the balance between U supply and reduction rates both in the laboratory[5] and in natural environments[11,20]. For the latter, it is commonly assumed that the delivery of U to the sediment is diagenetically controlled[11,20–22]. It is considered that diffusion-limited conditions in the sediment pore water result in U depletion, such that the intrinsic fractionation factor is not fully expressed[11]. Such U supply limiting conditions may occur in particular in restricted basins with high productivity or with large organic carbon inputs, leading to anoxia and increased U reaction rates. Indeed, high reduction rates result in the depletion of U ("reservoir effect"), dampening the effective observed isotope fractionation[11,21,22]. Most studies modeling U isotope fractionation in such systems (e.g., Andersen et al. [11]) assume an intrinsic fractionation factor derived from laboratory microbial reduction experiments (i.e., ~1.2‰) in which full expression of the fractionation is possible[6,8,9].

However, given that isotope signatures are not only dependent on the extent of the reduction, but on the reaction mechanism that generated them, consideration should be given not only to the balance between U supply and reduction[5,7], but to reaction free energy[29,38] and electron flux to and from the reductant (this study). Indeed, our data suggest an additional role for a physiological component, whereby increases in organic carbon inputs (electron donor) may suppress the intrinsic fractionation factor itself (from ~1‰ to values approaching 0‰), independent of U transport effects. To this end, further work is required to assess how fractionation factors are impacted by the type and availability of carbon, the bacterial species, and endogenous effects, such as competing pathways and protein expression levels within the electron transport chain.

Such data may permit organic carbon availability (e.g., in black shales) to be related to an intrinsic fractionation factor that considers microbial electron flux. In turn, incorporation of this parameter may further constrain modern frameworks of U isotope systematics and ultimately improve reconstructions of paleo ocean anoxia. For instance, a recent study has reported a negative correlation between total organic carbon (TOC) and authigenic U $\delta^{238}U$ in Mediterranean sapropels[50] at higher TOC concentrations (>2.5 wt. %). The occurrence of the maximum fractionation at intermediate TOC values was interpreted as being due to the contribution of both a non-diffusion-limited process for U reduction (resulting in high fractionation) and a diffusion-limited process (associated with a low fractionation). Alternatively, such a finding is also consistent with high TOC driving a high biological electron flux resulting in incomplete expression of U isotope fractionation and a lower intrinsic isotope fractionation factor (as shown in this study). We posit that biological electron flux (and by extension bioavailable organic carbon as an electron donor) needs to be considered as a factor impacting U isotopic fractionation in sedimentary environments. In particular, scenarios in which limited expression of U isotope fractionation is observed may have to be re-examined.

Methods

Culturing of *Shewanella oneidensis* MR-1. *Shewanella oneidensis* MR-1 was routinely grown in oxic Luria-Bertani (LB) medium to mid-late exponential phase. Cultures were then harvested by centrifugation for 10 min at 5000 × *g* and washed in a sterile anoxic buffer containing 30 mM sodium bicarbonate and 20 mM piperazine-N,N′-bis(2-ethanesulfonic acid) (PIPES) at pH 7.3. The washed cells were then resuspended and washed with either an anoxic 5 mM sodium citrate or 5 mM sodium EDTA solution, with 20 mM PIPES at pH 7. Finally, the cultures were resuspended in the same medium to an appropriate density, prior to addition to experimental reactors.

Reduction of U^{VI} by *S. oneidensis* MR-1. Anoxic reactors containing either 5 mM sodium citrate or 5 mM sodium EDTA and 20 mM PIPES at pH 7 were prepared. 20 mM sodium lactate was supplied as the electron donor, except for the experiments concerning variable lactate concentrations, for which lactate was supplied from a concentrated stock. All experimental media was autoclaved, flushed with pure and sterile N_2 for several hours, and then stored in the dark at ~25 °C inside an anoxic chamber (100% N_2, <0.1 ppm O_2; MBraun, Germany). 200 μM U^{VI} was added from an anoxic ~20 mM IRMM-184 U chloride stock. Aliquots of the *S. oneidensis* MR-1 cell suspensions were then added to the reactors to give a final optical density of 1, as measured at 600 nm (OD_{600nm}) using a UV-Vis spectrophotometer, which was equivalent to approximately 5×10^8 cells mL^{-1}. For the experiments concerning variable biomass concentrations, the cell suspensions were diluted to give final biomass concentrations of 0.1, 0.3, 1, and 3 (OD_{600nm}), corresponding to 0.23×10^8, 0.7×10^8, 2.3×10^8 and 11×10^8 cells mL^{-1} respectively. Abiotic control

experiments did not display reduction of U^{VI} (Supplementary Figs. 9 and 10).

Preparation of a CFE. *S. oneidensis* MR-1 was grown anaerobically in LB medium, followed by centrifugation for 10 min at 8000 × *g* and 4 °C. The cells were then washed twice in sterile anoxic 5 mM sodium citrate with 20 mM PIPES at pH 7. The cell suspension was transferred to a French press under anoxic conditions and pressed at 6894.8 kPa (~1000 psi) for three cycles. The solution containing the lysed cells was then collected and centrifuged for 10 min at 8000 × *g* and 4 °C in order to remove any cell membrane debris. The supernatant containing the CFE was then filtered through a 0.2 µm filter and the solution was diluted such that the CFE was the equivalent product of whole cells at a concentration of $OD_{600nm} = 1$ (approximately 5×10^8 cells mL^{-1}), giving a final protein concentration of 272 µg mL^{-1}. The presence of reduced cytochromes was confirmed by UV-Vis spectrophotometry.

Reduction of U^{VI} by CFE. As for whole cells, 200 µM U^{VI} was added from an anoxic stock, and the reactors were incubated in the dark inside an anoxic chamber.

Purification of MtrC. Recombinant, soluble, His-tagged MtrC was expressed in the Δ*omc*Δ*mtrC* strain of *S. oneidensis* MR-1 LS331, kindly supplied by Liang Shi[51]. First, 5 to 10 L cultures were grown overnight in LB broth at 30 °C, and expression of the soluble MtrC was induced with 0.1 mM L-arabinose. The whole cells were then removed by centrifugation for 30 min at 5000 × *g* and the MtrC-containing supernatant was loaded onto 5 mL HisTrap EXCEL columns prepacked with Ni Sepharose with a flow rate of 5–6 mL min^{-1}. The protein was then eluted with 40 mM imidazole and 150 mM NaCl, concentrated to 5 mL, and loaded onto a HiLoad 16/600 Superdex 200 size exclusion chromatography column that had been pre-conditioned with 150 mM NaCl and 20 mM HEPES at pH 7.5. The peak fractions were collected, pooled, and concentrated, and SDS-PAGE indicated the presence of a single band at ~75 kDa, confirming the successful purification. The final protein concentration was determined colorimetrically via the bicinchoninic acid assay (Pierce™ BCA Protein Assay Kit, ThermoFisher Scientific, Waltham MA USA).

Reduction of MtrC. The purified MtrC was transferred to an anoxic chamber and chemically reduced via step-wise addition of a 10 mM sodium dithionite solution ($Na_2S_2O_4$). Between additions, the heme redox status was monitored via UV-Vis spectrophotometry at a wavelength of 500 to 580 nm (UV-2501P, Shimadzu, Kyoto Japan). Oxidized MtrC displays a broad peak with a maximum of 530 nm, whereas reduced MtrC displays two characteristic peaks at 522 nm and 552 nm (β and α Soret absorption peaks). For the preparation of a fully-reduced MtrC, sodium dithionite was successively added until no further change in the UV-Vis spectrum was observed, and the added quantity was then noted. Partially-reduced MtrC was then prepared by the addition of approximately 40% of the sodium dithionite required to completely reduce MtrC. Any excess sodium dithionite was then removed from both preparations by dialysis in 50 mM NaCl and 100 mM HEPES at pH 7. Dialysis cassettes (0.5 mL Side-A-Lyzer, ThermoFisher Scientific, Waltham MA, USA) were loaded with the protein and left in 500 mL of dialysis buffer for 18 h inside the anoxic chamber. Once complete, aliquots of each preparation were stored at −20 °C inside the anoxic chamber until required. Oxidized MtrC was treated in the same manner, except for the addition of sodium dithionite.

Reduction of U^{VI}-EDTA by chemically reduced MtrC. Reactors containing 150 µM U^{VI}, 5 mM sodium EDTA, 50 mM NaCl, and 100 mM HEPES at pH 7 were prepared inside an anoxic chamber. U^{VI} reduction was initiated by the addition of either 67 µM fully-reduced MtrC or 117 µM partially-reduced MtrC.

Reaction of oxidized MtrC with U^{IV}-EDTA. U^{IV}-EDTA was generated via the reduction of U^{VI}-EDTA by *S. oneidensis* MR-1, as described above. This reaction was left for at least one week before filtering through a 0.2 µm filter to remove the biomass. Then an aliquot of oxidized MtrC was added to give a final concentration of ~150 µM U and 150 µM MtrC. After approximately 1 h, an aliquot was removed and the heme redox status was measured using a UV-vis spectrophotometer. The U oxidation state was then determined via ion exchange chromatography (see below).

Ion Exchange Chromatography. As reduction of U^{VI} in the presence of either 5 mM citrate or EDTA results in both a soluble reactant and product (Supplementary Figs. 1, 3, 4, 5, and 10), U^{VI} concentrations and isotopic signatures in all reactions were monitored by first separating U^{VI} from the total U using an anion exchange chromatography protocol adapted from the one described by Stoliker et al. [52,53]. Strongly basic anion exchange resin (Dowex 1 × 8; 100 − 200 mesh) was added to polypropylene columns to give a bed volume of 2.5 mL. The resin was pre-conditioned with 4.5 N HCl and then loaded with 50 µL of U containing sample that had been acidified to 4.5 N HCl. The U^{IV} fraction was eluted by the addition of 10 successive bed volumes of 4.5 N HCl. The U^{VI} was then eluted with 10 bed volumes of 0.1 N HCl. Ultrapure reagents were used throughout and all steps were performed inside an anoxic chamber with solutions that were flushed with nitrogen for more than 2 h before use. After separation, U concentrations were measured via ICP-MS.

This procedure has also been successfully applied to the measurement of U^{VI} and U^{IV} isotope signatures[43,54]. Whilst these previous studies observed cross contamination between the two oxidation states and thus applied a correction factor to the measured $\delta^{238}U$, negligible cross-contamination was observed during our own tests under the conditions described below. Hence, no correction factor was applied.

U isotope ratio analysis. Samples were first weighed and evaporated to dryness. The samples were then treated with a mixture of 200 µL 14 M HNO_3 and 200 µL H_2O_2 (30 %) to destructively oxidize organic materials. Uranium was then purified by ion-exchange chromatography according to a method described by Weyer et al. [13]. The samples were dissolved in 1 mL 3 M HNO_3 and U was purified on Eichrom UTEVA resin. Prior to the chemical separation, a weighed aliquot of the $^{236}U/^{233}U$ double spike solution (IRMM 3636-A, $^{236}U/^{233}U = 0.98130$) was added to the samples in order to correct for isotope fractionation during U purification and instrumental mass discrimination during MC-ICP-MS analysis. Spike/sample mixtures for all samples and standards were adjusted to similar ratios ($^{236}U/^{235}U \approx 3 \pm 10\%$) to minimize peak tailing effects (from the ion beams of ^{238}U on ^{236}U and of ^{236}U on ^{235}U).

U isotope measurements were performed at Leibniz Universität Hannover with a Thermo-Finnigan Neptune multi-collector ICP-MS (MC-ICP-MS), similar to the protocol published by Noordman et al. [55]. For sample introduction, a Cetac Aridus-II desolvation system equipped with a perfluoroalkoxy alkane (PFA) nebulizer with a sampling rate of 100 µL/min was used to enhance sensitivity and to reduce solvent-based interferences such as oxides and hydrides. Additionally, a standard Ni sampling cone

and a Ni X skimmer cone were used in combination with a 0.8 mm copper ring (spacer). With this setup, a 70 ng/g solution achieved a ~70 V signal on ^{238}U in low mass resolution mode.

The abundance sensitivity was determined before each analysis term and was typically ≤0.1 ppm of the ^{238}U signal at mass 236 (determined on a spike-free solution), resulting in negligible tail correction.

All samples and standards were measured with ~4 min total integration time and mass bias correction was performed with the IRMM 3636-A double spike[56] and the exponential law[57]. A standard sample bracketing method was applied during analysis, i.e., two sample measurements were bracketed by two standard measurements. The results for all sample analyses are presented in the delta notation relative to the IRMM-184 U standard:

$$\delta^{238}U = \left[\frac{(^{238}U/^{235}U)_{sample}}{(^{238}U/^{235}U)_{standard}} - 1\right] \cdot 1000[‰]$$

Each sample was analyzed three times and the precision is given as two standard deviations (2 S.D.) of the replicate analysis for each sample (typically ≤ 0.1‰). Additionally, reproducibility and accuracy were determined by replicate analyses of the U-standards IRMM-184 and REIMEP 18-A relative to CRM −112A during each analysis session and the results agreed with those previously reported in the literature, within uncertainty[13,22,55,56].

Rayleigh distillation models. Isotope fractionation factors for a given reaction were determined by fitting Rayleigh distillation models to the measured isotopic signatures, according to the method described in Scott et al. [58] and using the following formula:

$$\delta_t = (\delta_0 + 1000‰)\left[\frac{c_t}{c_0}\right]^{\alpha-1} - 1000‰$$

where c_0 and δ_0 are the initial concentration and isotopic composition of U^{VI}, and c_t and δ_t are the concentration and isotopic composition of U^{VI} at time t. The fractionation factors (ε) were obtained from the slope (α–1) of the linear regression of the experimental data in linearized plots of $\ln(\delta^{238}U + 1000‰)$ versus $\ln(c_t/c_0)$, where $\varepsilon = (\alpha–1)\times1000$.

Reporting summary. Further information on research design is available in the Nature Portfolio Reporting Summary linked to this article.

Data availability

All relevant data are available in a repository at https://doi.org/10.5281/zenodo.7636182 [59], or on request from the authors.

Received: 24 February 2023; Accepted: 5 September 2023;
Published online: 19 September 2023

References

1. Andersen, M. B., Stirling, C. H. & Weyer, S. Uranium isotope fractionation. *Rev. Mineral. Geochem.* **82**, 799–850 (2017).
2. Brennecka, G. A., Herrmann, A. D., Algeo, T. J. & Anbar, A. D. Rapid expansion of oceanic anoxia immediately before the end-Permian mass extinction. *Proc. Natl. Acad. Sci. USA.* **108**, 17631–17634 (2011).
3. Montoya-Pino, C. et al. Global enhancement of ocean anoxia during Oceanic Anoxic Event 2: a quantitative approach using U isotopes. *Geology* **38**, 315–318 (2010).
4. Lau, K. V. et al. Marine anoxia and delayed Earth system recovery after the end-Permian extinction. *Proc. Natl. Acad. Sci. USA.* **113**, 2360–2365 (2016).
5. Basu, A. et al. Microbial U isotope fractionation depends on U(VI) reduction rate. *Environ. Sci. Technol.* **54**, 2295–2303 (2020).
6. Basu, A., Sanford, R. A., Johnson, T. M., Lundstrom, C. C. & Löffler, F. E. Uranium isotopic fractionation factors during U(VI) reduction by bacterial isolates. *Geochim. Cosmochim. Acta* **136**, 100–113 (2014).
7. Brown, S. T., Basu, A., Ding, X., Christensen, J. N. & DePaolo, D. J. Uranium isotope fractionation by abiotic reductive precipitation. *Proc. Natl. Acad. Sci. USA.* **115**, 8688–8693 (2018).
8. Stylo, M. et al. Uranium isotopes fingerprint biotic reduction. *Proc. Natl. Acad. Sci. USA.* **112**, 5619–5624 (2015).
9. Stirling, C. H., Andersen, M. B., Warthmann, R. & Halliday, A. N. Isotope fractionation of ^{238}U and ^{235}U during biologically-mediated uranium reduction. *Geochim. Cosmochim. Acta* **163**, 200–218 (2015).
10. Bopp, C. J. et al. Uranium 238U/235U isotope ratios as indicators of reduction: results from an in situ biostimulation experiment at Rifle, Colorado, U.S.A. *Environ. Sci. Technol.* **44**, 5927–5933 (2010).
11. Andersen, M. B. et al. A modern framework for the interpretation of $^{238}U/^{235}U$ in studies of ancient ocean redox. *Earth Planet. Sci. Lett.* **400**, 184–194 (2014).
12. Stirling, C. H., Andersen, M. B., Potter, E.-K. & Halliday, A. N. Low-temperature isotopic fractionation of uranium. *Earth Planet. Sci. Lett.* **264**, 208–225 (2007).
13. Weyer, S. et al. Natural fractionation of $^{238}U/^{235}U$. *Geochim. Cosmochim. Acta* **72**, 345–359 (2008).
14. Abe, M., Suzuki, T., Fujii, Y., Hada, M. & Hirao, K. An ab initio molecular orbital study of the nuclear volume effects in uranium isotope fractionations. *J. Chem. Phys* **129**, 164309 (2008).
15. Schauble, E. A. Role of nuclear volume in driving equilibrium stable isotope fractionation of mercury, thallium, and other very heavy elements. *Geochim. Cosmochim. Acta* **71**, 2170–2189 (2007).
16. Bigeleisen, J. Nuclear size and shape effects in chemical reactions. Isotope chemistry of the heavy elements. *J. Am. Chem. Soc* **118**, 3676–3680 (1996).
17. Moynier, F., Fujii, T., Brennecka, G. A. & Nielsen, S. G. Nuclear field shift in natural environments. *Comptes Rendus - Geosci* **345**, 150–159 (2013).
18. Fujii, T., Moynier, F. & Albarède, F. The nuclear field shift effect in chemical exchange reactions. *Chem. Geol.* **267**, 139–156 (2009).
19. Rademacher, L. K. et al. Experimentally determined uranium isotope fractionation during reduction of hexavalent U by bacteria and zero valent iron. *Environ. Sci. Technol.* **40**, 6943–6948 (2006).
20. Lau, K. V., Lyons, T. W. & Maher, K. Uranium reduction and isotopic fractionation in reducing sediments: Insights from reactive transport modeling. *Geochim. Cosmochim. Acta* **287**, 65–92 (2020).
21. Lau, K. V. et al. Variable local basin hydrography and productivity control the uranium isotope paleoredox proxy in anoxic black shales. *Geochim. Cosmochim. Acta* **317**, 433–456 (2022).
22. Brüske, A. et al. Correlated molybdenum and uranium isotope signatures in modern anoxic sediments: Implications for their use as paleo-redox proxy. *Geochim. Cosmochim. Acta* **270**, 449–474 (2020).
23. Rolison, J. M., Stirling, C. H., Middag, R. & Rijkenberg, M. J. A. Uranium stable isotope fractionation in the Black Sea: modern calibration of the $^{238}U/^{235}U$ paleo-redox proxy. *Geochim. Cosmochim. Acta* **203**, 69–88 (2017).
24. Lefebvre, P. et al. Isotopic fingerprint of uranium accumulation and redox cycling in floodplains of the Upper Colorado River Basin. *Environ. Sci. Technol.* **53**, 3399–3409 (2019).
25. Lovley, D. R., Phillips, E. J. P., Gorby, Y. A. & Landa, E. R. Microbial reduction of uranium. *Nature* **350**, 413–416 (1991).
26. Wall, J. D. & Krumholz, L. R. Uranium reduction. *Annu. Rev. Microbiol.* **60**, 149–166 (2006).
27. Shi, L. et al. Extracellular electron transfer mechanisms between microorganisms and minerals. *Nat. Rev. Microbiol.* **14**, 651–662 (2016).
28. Marshall, M. J. et al. *c*-type cytochrome-dependent formation of U(IV) nanoparticles by *Shewanella oneidensis*. *PLoS Biol* **4**, 1324–1333 (2006).
29. Joe-Wong, C. & Maher, K. A model for kinetic isotope fractionation during redox reactions. *Geochim. Cosmochim. Acta* **269**, 661–677 (2020).
30. Wang, H. et al. Metabolomic analyses show that electron donor and acceptor ratios control anaerobic electron transfer pathways in *Shewanella oneidensis*. *Metabolomics* **9**, 642–656 (2013).
31. Kouzuma, A., Kasai, T., Hirose, A. & Watanabe, K. Catabolic and regulatory systems in *Shewanella oneidensis* MR−1 involved in electricity generation in microbial fuel cells. *Front. Microbiol.* **6**, 609 (2015).
32. Li, F. et al. Modular engineering intracellular NADH regeneration boosts extracellular electron transfer of *Shewanella oneidensis* MR-1. *ACS Synth. Biol.* **7**, 885–895 (2018).
33. Luo, S., Guo, W., Nealson, K. H., Feng, X. & He, Z. ^{13}C pathway analysis for the role of formate in electricity generation by *Shewanella Oneidensis* MR−1 using lactate in microbial fuel cells. *Sci. Rep.* **6**, 20941 (2016).
34. Ishiki, K. & Shiigi, H. Kinetics of intracellular electron generation in *Shewanella oneidensis* MR−1. *Anal. Chem.* **91**, 14401–14406 (2019).

35. Brunner, B. & Bernasconi, S. M. A revised isotope fractionation model for dissimilatory sulfate reduction in sulfate reducing bacteria. *Geochim. Cosmochim. Acta* **69**, 4759–4771 (2005).
36. Rees, C. E. A steady-state model for sulphur isotope fractionation in bacterial reduction processes. *Geochim. Cosmochim. Acta* **37**, 1141–1162 (1973).
37. Sato, A., Bernier-Latmani, R., Hada, M. & Abe, M. Ab initio and steady-state models for uranium isotope fractionation in multi-step biotic and abiotic reduction. *Geochim. Cosmochim. Acta* **307**, 212–227 (2021).
38. Joe-Wong, C., Weaver, K. L., Brown, S. T. & Maher, K. Thermodynamic controls on redox-driven kinetic stable isotope fractionation. *Geochemical Perspect. Lett*. 20–25 https://doi.org/10.7185/geochemlet.1909 (2019).
39. Molinas, M. et al. Biological reduction of a U(V)-organic ligand complex. *Environ. Sci. Technol.* **55**, 4753–4761 (2021).
40. Vettese, G. F. et al. Multiple lines of evidence identify U(V) as a key intermediate during U(VI) reduction by *Shewanella oneidensis* MR1. *Environ. Sci. Technol.* **54**, 2268–2276 (2020).
41. Molinas, M., Meibom, K. L., Faizova, R., Mazzanti, M. & Bernier-Latmani, R. Mechanism of reduction of aqueous U(V)-dpaea and solid-phase U(VI)-dpaea complexes: The role of multiheme *c*-type cytochromes. *Environ. Sci. Technol.* **57**, 7537–7546 (2023).
42. Berry, E. A. & Trumpower, B. L. Simultaneous determination of hemes *a*, *b*, and *c* from pyridine hemochrome spectra. *Anal. Biochem.* **161**, 1–15 (1987).
43. Wang, X., Johnson, T. M. & Lundstrom, C. C. Isotope fractionation during oxidation of tetravalent uranium by dissolved oxygen. *Geochim. Cosmochim. Acta* **150**, 160–170 (2015).
44. Hartshorne, R. S. et al. Characterization of an electron conduit between bacteria and the extracellular environment. *Proc. Natl. Acad. Sci. USA.* **106**, 22169–22174 (2009).
45. Yang, S. & Liu, Y. Nuclear field shift effects on stable isotope fractionation: a review. *Acta Geochim* **35**, 227–239 (2016).
46. Bigeleisen, J. & Wolfsberg, M. Theoretical and experimental aspects of isotope effects in chemical kinetics. in *Advances in Chemical Physics* (eds. Prigogine, I. & Debye, P.) 15–76 (John Wiley & Sons, Inc., 1957). https://doi.org/10.1002/9780470143476.ch2.
47. Bradley, A. S. et al. Patterns of sulfur isotope fractionation during microbial sulfate reduction. *Geobiology* **14**, 91–101 (2016).
48. Sim, M. S., Ono, S., Donovan, K., Templer, S. P. & Bosak, T. Effect of electron donors on the fractionation of sulfur isotopes by a marine *Desulfovibrio* sp. *Geochim. Cosmochim. Acta* **75**, 4244–4259 (2011).
49. Wing, B. A. & Halevy, I. Intracellular metabolite levels shape sulfur isotope fractionation during microbial sulfate respiration. *Proc. Natl. Acad. Sci. USA.* **111**, 18116–18125 (2014).
50. Clarkson, M. O. et al. Environmental controls on very high δ238U values in reducing sediments: Implications for Neoproterozoic seawater records. *Earth-Science Rev* **237**, 104306 (2023).
51. Shi, L. et al. Isolation of a high-affinity functional protein complex between OmcA and MtrC: Two outer membrane decaheme *c*-type cytochromes of *Shewanella oneidensis* MR-1. *J. Bacteriol.* **188**, 4705–4714 (2006).
52. Stoliker, D. L. et al. Evaluating chemical extraction techniques for the determination of uranium oxidation state in reduced aquifer sediments. *Environ. Sci. Technol.* **47**, 9225–9232 (2013).
53. Stoliker, D. L., Kaviani, N., Kent, D. B. & Davis, J. A. Evaluating ion exchange resin efficiency and oxidative capacity for the separation of uranium(IV) and uranium(VI). *Geochem. Trans.* **14**, 1 (2013).
54. Wang, X., Johnson, T. M. & Lundstrom, C. C. Low temperature equilibrium isotope fractionation and isotope exchange kinetics between U(IV) and U(VI). *Geochim. Cosmochim. Acta* **158**, 262–275 (2015).
55. Noordmann, J. et al. Uranium and molybdenum isotope systematics in modern euxinic basins: Case studies from the central Baltic Sea and the Kyllaren fjord (Norway). *Chem. Geol.* **396**, 182–195 (2015).
56. Richter, S. et al. New average values for the n(238U)/n(235U) isotope ratios of natural uranium standards. *Int. J. Mass Spectrom.* **295**, 94–97 (2010).
57. Russell, W. A., Papanastassiou, D. A. & Tombrello, T. A. Ca isotope fractionation on the Earth and other solar system materials. *Geochim. Cosmochim. Acta* **42**, 1075–1090 (1978).
58. Scott, K. M., Lu, X., Cavanaugh, C. M. & Liu, J. S. Optimal methods for estimating kinetic isotope effects from different forms of the Rayleigh distillation equation. *Geochim. Cosmochim. Acta* **68**, 433–442 (2004).
59. Brown, A. R. *et al*. Electron flux is a key determinant of uranium isotope fractionation during bacterial reduction. *Zenodo* https://doi.org/10.5281/zenodo.7636182 (2023).

Acknowledgements

We thank Liang Shi for providing the recombinant MtrC *S. oneidensis* LS331 strain and Florence Pojer, Kelvin Lau and Amédé Larabi of the Protein Production and Structure Core Facility at EPFL for purification of MtrC. We also acknowledge Camila Morales for assistance with experiments and Prof. Masahiko Hada of Tokyo Metropolitan University for helpful discussions. Funding for this work was provided by an ERC consolidator grant awarded to R. Bernier-Latmani (725675: UNEARTH: "Uranium isotope fractionation: a novel biosignature to identify microbial metabolism on early Earth"). This work was also supported by JSPS KAKENHI Grant Numbers JP21H01864 and JP22J12551.

Author contributions

R.B.-L., S.W., M.A., A.R.B. and M.M. designed research; A.R.B., Y.R. performed research, A.R.B., Y.R., S.W. and R.B.-L. analyzed data; and A.R.B., M.M., Y.R., A.S., M.A., S.W. and R.B.-L. wrote the manuscript.

Competing interests

The authors declare no competing interests.

Additional information

Supplementary information The online version contains supplementary material available at https://doi.org/10.1038/s43247-023-00989-x.

Correspondence and requests for materials should be addressed to Rizlan Bernier-Latmani.

Peer review information *Communications Earth & Environment* thanks Geoffrey J. Gilleaudeau and the other, anonymous, reviewer(s) for their contribution to the peer review of this work. Primary Handling Editors: Mojtaba Fakhraee and Joe Aslin. A peer review file is available.

Reprints and permission information is available at http://www.nature.com/reprints

Publisher's note Springer Nature remains neutral with regard to jurisdictional claims in published maps and institutional affiliations.